ADVANCED MATERIALS TECHNOLOGIES
www.advmattechnol.de

Highly Adaptive and Sustainable Oil Purification Driven by Triboelectric Nanogenerator

Xingfu Wan, Minzheng Sun, Zongchen Su, Fangming Li, and Minyi Xu**

Oil contamination poses a critical challenge in mechanical systems, leading to significant degradation in oil performance, and adversely affecting machinery operation and longevity. This study introduces an innovative electrostatic oil purification method based on a freestanding rotary triboelectric nanogenerator (FR-TENG). By harnessing ambient mechanical energy, the FR-TENG generates a high-voltage electric field, which induces electrostatic forces on solid contaminants, causing them to migrate and adhere to the dust collector. Multi-physics simulations are utilized to investigate the purification dynamics and explore the underlying mechanisms, providing a comprehensive understanding of the process. Experiments further confirm that this method is highly effective in removing solid particles from oil with high moisture content while dehydrating the oil. Compared to traditional electrostatic purification methods, which require moisture levels below 1000 ppm, the method maintains high purification efficiency even with oil containing up to 10% moisture content, extending the permissible moisture limit by nearly 100-fold. These findings highlight the significant potential of this highly adaptive and sustainable technique for oil purification, allowing for simultaneous efficient particle purification and dehydration even in scenarios with high moisture contamination. Thus paving the way for broader applications of TENG technology in industrial oil treatment.

1. Introduction

In modern industrial systems, oils fulfill crucial functions, including sealing, lubrication, cooling, wear mitigation, and hydraulic transmission in mechanical equipment.[1–3] However, equipment operation inevitably introduces contaminants into the oil, such as metal abrasives, oxidation products, dust, and water,[4] which cause most machinery failures. Therefore, removing contaminants is essential for reducing machinery failures and lowering failure rates, thus extending the service life of both oils and equipment.[5–7] Currently, mainstream oil purification methods are broadly categorized as density gradient separation, filtration, adsorption, and electrostatic oil purification. Density-based separation techniques, such as gravity settling and centrifugal separation, are ineffective in removing contaminants with densities similar to the oil, limiting their applicability to preliminary purification stages. The separation efficiency of filtration depends on the precision of the filter membrane. However, a higher precision membrane entails greater energy consumption and increased susceptibility to clogging.[8,9] Adsorption is simple to operate, but it can only selectively remove contaminants and may lead to secondary pollution.[10] Electrostatic oil purification utilizes an externally applied electric field with a gradient and can remove the majority of contaminants from the oil,[11] particularly demonstrating significant purification effects on submicron-level contaminants.[12] However, due to the high sensitivity of high-voltage electric fields to moisture, this method can only be employed in oils with extremely low moisture content. Therefore, there is an urgent need to discover a highly efficient, reliable, adaptable, and sustainable oil purification method.

In 2012, Wang et al. proposed the Triboelectric Nanogenerator (TENG), a high-voltage capacitive power source.[13,14] It operates on the triboelectric effect, which encompasses contact electrification and electrostatic induction to achieve the conversion of external mechanical stimuli into electrical signals.[15–17] Such nanogenerators exhibit significant application potential in environmental energy harvesting, self-powered sensors, and self-sustaining systems.[18–20] Among various TENGs, the freestanding TENG is capable of converting external linear stimuli into rotational motion, achieving continuous high-voltage output within limited space.[21] It exhibits a high optimal matching impedance, making it suitable for driving high-impedance applications.[22–26] Compared to traditional high-voltage power sources, FR-TENG offers advantages such as portability, safety, and self-powering capability.[27,28] In recent years, applications have expanded to include electrospinning,[29,30] air purification,[31,32] disinfection,[33,34] oil-water separation,[35] and dielectric elastomer driving.[36] In particular, Lei et al. employed a charge accumulation strategy to elevate the output voltage of the TENG to 20 kV and proposed its application in self-powered oil purification systems.[37] Qu et al. conducted triboelectric

X. Wan, M. Sun, Z. Su, F. Li, M. Xu
State Key Laboratory of Maritime Technology and Safety
Marine Engineering College
Dalian Maritime University
Dalian 116026, China
E-mail: lifangming@dlmu.edu.cn; xuminyi@dlmu.edu.cn

The ORCID identification number(s) for the author(s) of this article can be found under https://doi.org/10.1002/admt.202401773

DOI: 10.1002/admt.202401773

charging on impurity particles before electrostatic oil purification to enhance its efficiency.[38] Li et al. successfully applied FR-TENG to dehydration in water-in-oil emulsions, increasing the applicable moisture content for electric dehydration to 60%. This indicates the capability of TENG to handle water-containing oil.[39] Traditional electrostatic oil purifiers require the application of a direct current (DC) voltage of tens of kilovolts to separate pollutants, necessitating that the moisture content of the oil remains below 1000 ppm. Otherwise, it could lead to severe short-circuit current damage.[40,41] Due to the limited internal capacitance of TENG, the moisture-induced short-circuit hazards are effectively mitigated by limited energy surge, thus the short-circuit protection by TENG is provided. Therefore, TENG demonstrates significant potential for the effective treatment of contaminants in oil with high moisture content.

In this work, a self-powered triboelectric electrostatic oil purifier (TEOP) is proposed. The FR-TENG serves as a power source for the TEOP, providing high-voltage electricity while harvesting ambient energy. Utilizing ambient energy, the FR-TENG generates an electric field for purification. To further understand the purification mechanism, a multi-physics field coupling model is developed to simulate the dynamic migration of impurities under the influence of a direct current non-uniform electric field. Experimental and simulation results consistently demonstrate the superior purification performance of the TEOP, showing a significant reduction in both solid contaminants and water content in oil samples. Notably, this system can be driven by the wind energy harvested by a turbine mounted on the FR-TENG rotor, making it suitable for industrial applications where renewable energy can be utilized. These findings highlight the robustness and adaptability of TEOP for oil purification in different environments, opening up new avenues for the application of triboelectric nanogenerators in sustainable energy-driven oil purification systems.

2. Results and Discussion

2.1. Structure and Working Principle of TEOP

The configuration of the FR-TENG is illustrated in **Figure 1a**, wherein the stator component consists of a pair of grid electrodes fabricated on a Printed Circuit Board (PCB). The electrode is covered with nylon film, and each electrode is subdivided into six segments. The rotor component comprises an acrylic disk serving as the rotating element, affixed with polyvinyl chloride (PVC) film. Upon assembly of the rotor and stator, the PVC film maintains constant contact with the nylon film due to both the compression force and the inherent plasticity of PVC.

Figure 1b shows the schematic diagram of the TEOP, which comprises the FR-TENG, the purifier, and a half-wave voltage doubler circuit. Impurities present in oil typically acquire an electrical charge through collision, friction, or charge injection. TEOP can harness wind energy through the TENG to generate an electric field with sufficient strength to propel impurities within the fluid. Consequently, these impurities migrate toward the center of the container, where they are adsorbed onto the dust collector.

Figure 1c illustrates the charge transfer process occurring within a single cycle of the FR-TENG and the general dynamic process of impurity particles during purification. As the rotor rotates, the contact and friction between the nylon and PVC film induce triboelectric charge transfer. Under the influence of electrostatic induction, the negative charges accumulated on the PVC film induce corresponding positive charges on the bottom electrodes, establishing an electric potential difference between the two electrodes. The rotational motion of the rotor propels the PVC film, generating alternating charge transfer across the electrodes. Subsequently, the alternating current (AC) is rectified into higher voltage DC power via a Power Management Circuit (PMC), which is connected to the electrodes within the purifier. This configuration establishes a DC field directed toward the center within the purifier. Consequently, impurities within the purifier are influenced by the electric field, causing them to migrate toward the center and be captured by the dust collector located outside the inner electrode. Smaller-diameter impurity particles can pass through the layers on the outside of the dust collector. However, the multi-layer structure of the dust collector ensures that smaller impurity particles can be effectively captured.

2.2. The Output and Characteristics of FR-TENG

To comprehensively evaluate the performance of the FR-TENG, a measurement circuit, as depicted in **Figure 2a**, was devised to assess its output. Given that the electrostatic meter's range is considerably smaller than the actual voltage values, the ammeter method was used for measurement. A standard large resistor was integrated into the circuit, and the voltage was determined by measuring the current within the resistor. The outcomes are illustrated in Figure 2b,c. We use a FR-TENG with an electrode spacing of 8 mm, resulting in an open-circuit voltage (V_{oc}) of 7.10 kV at 100 rpm, corresponding to a short-circuit current (I_{sc}) of 55.14 μA. As the rotational speed increases, V_{oc} exhibits a slight growth, accompanied by an increase in I_{sc}, peaking at 7.42 kV and 208.10 μA at 400 rpm.

To meet the electric field requirement for electrostatic oil purification, a half-wave voltage doubler was devised, as depicted in Figure 2d. The impact of this circuit on the open-circuit voltage at various rotational speeds is depicted in Figure 2e. Notably, at lower rotational speeds, the output voltage is diminished due to its dependency on the frequency of the input signal. The output voltage is determined by the following formula:[42]

$$V_{out} = 2nV_{oc} - \frac{V_{out}}{fCR}\left(\frac{2n^3}{3} + \frac{n^2}{2} - \frac{n}{6}\right) \quad (1)$$

where V_{out} Represents the output voltage of the circuit, n denotes the theoretical voltage multiplication factor of the circuit, f is the output frequency of the FR-TENG, C is the capacitance of the capacitor in the circuit, and R is the equivalent resistance of the load. At lower rotational speeds, the input signal frequency f is diminished, resulting in a substantial voltage drop across the circuit, thereby hindering the circuit's boosting effect from reaching the intended two-fold increase. However, as the rotational speed increases, the voltage drop diminishes, leading to an elevation in the output voltage until it eventually achieves a doubling effect. Figure 2f presents a comparison of the voltage output between the direct connection and the doubler at a given rotational

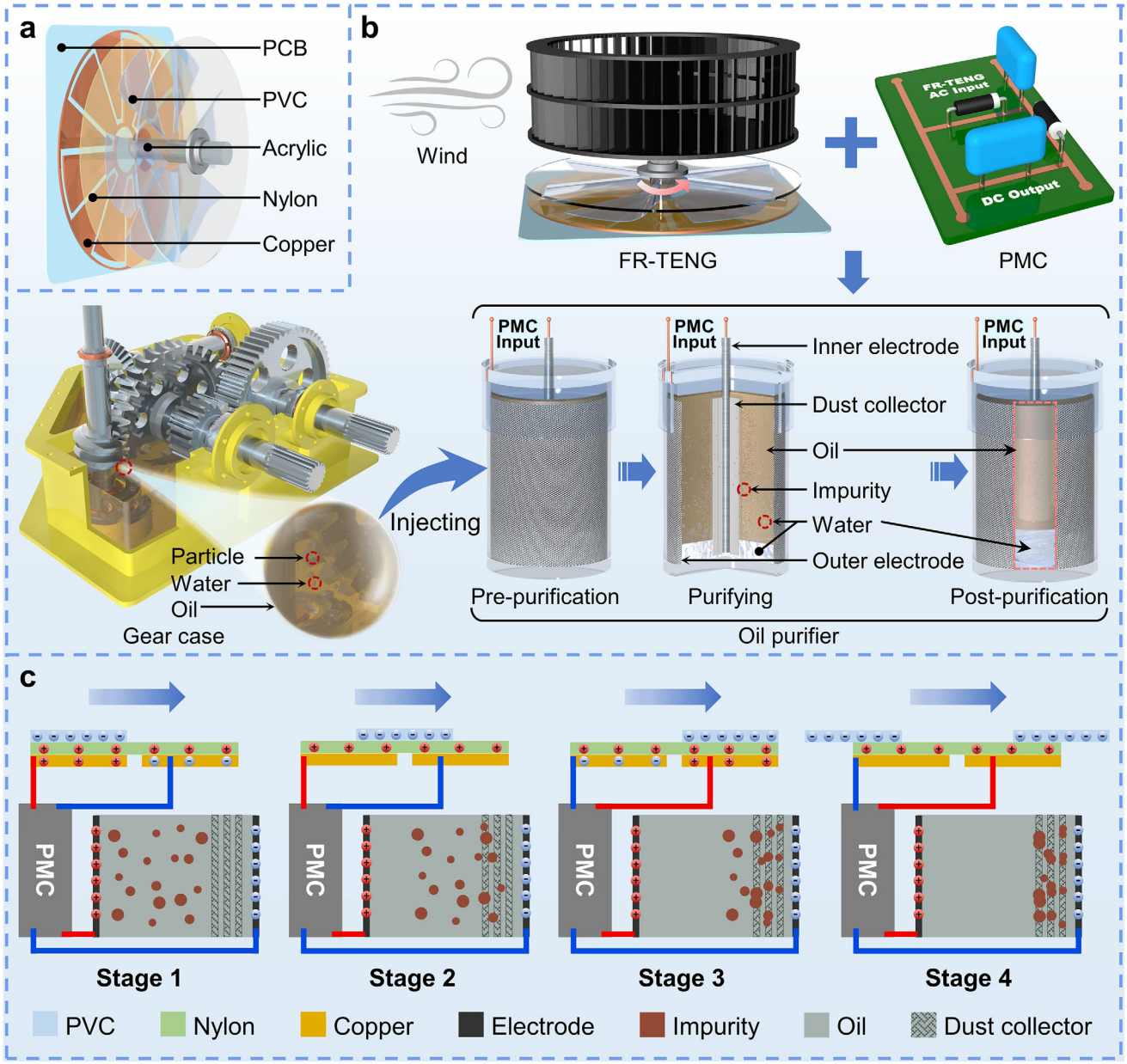

Figure 1. Design and Oil Purification Principle of TEOP. a) Structural diagram of FR-TENG. b) Schematic diagram of TEOP oil purification. c) Charge transfer process of FR-TENG in one cycle and corresponding impurity movement situation.

speed. At 100 rpm, the output voltage from the doubler is 6.76 kV due to excessive voltage drop, which is lower than direct connection. As the rotational speed increases, the voltage drop across the doubler diminishes, consequently elevating the output voltage. At 400 rpm, the output reaches 14.21 kV, thereby meeting the electric field requirements for effective oil purification.

Additionally, to prevent drastic humidity variations from affecting the output performance of the FR-TENG, a sealing treatment can be applied to the triboelectric layers of the FR-TENG.

Durability is equally crucial for FR-TENGs. To comprehensively evaluate the operational stability, we subjected the device to a rigorous durability test over 1000000 continuous cycles (at a rotational speed of 400 rpm). As depicted in Figure 2g, the FR-TENG exhibited limited voltage degradation overall. A relatively pronounced decline was observed during the first 150000 cycles, followed by minor fluctuations in subsequent cycles. The final output retained ≈90.94% of the initial value.

2.3. Simulation Analysis of the Oil Purification Process

The operation of mechanical equipment inevitably introduces solid impurities such as metal abrasive particles, carbon, dust, and oxides into the oil. The oil sample requiring purification

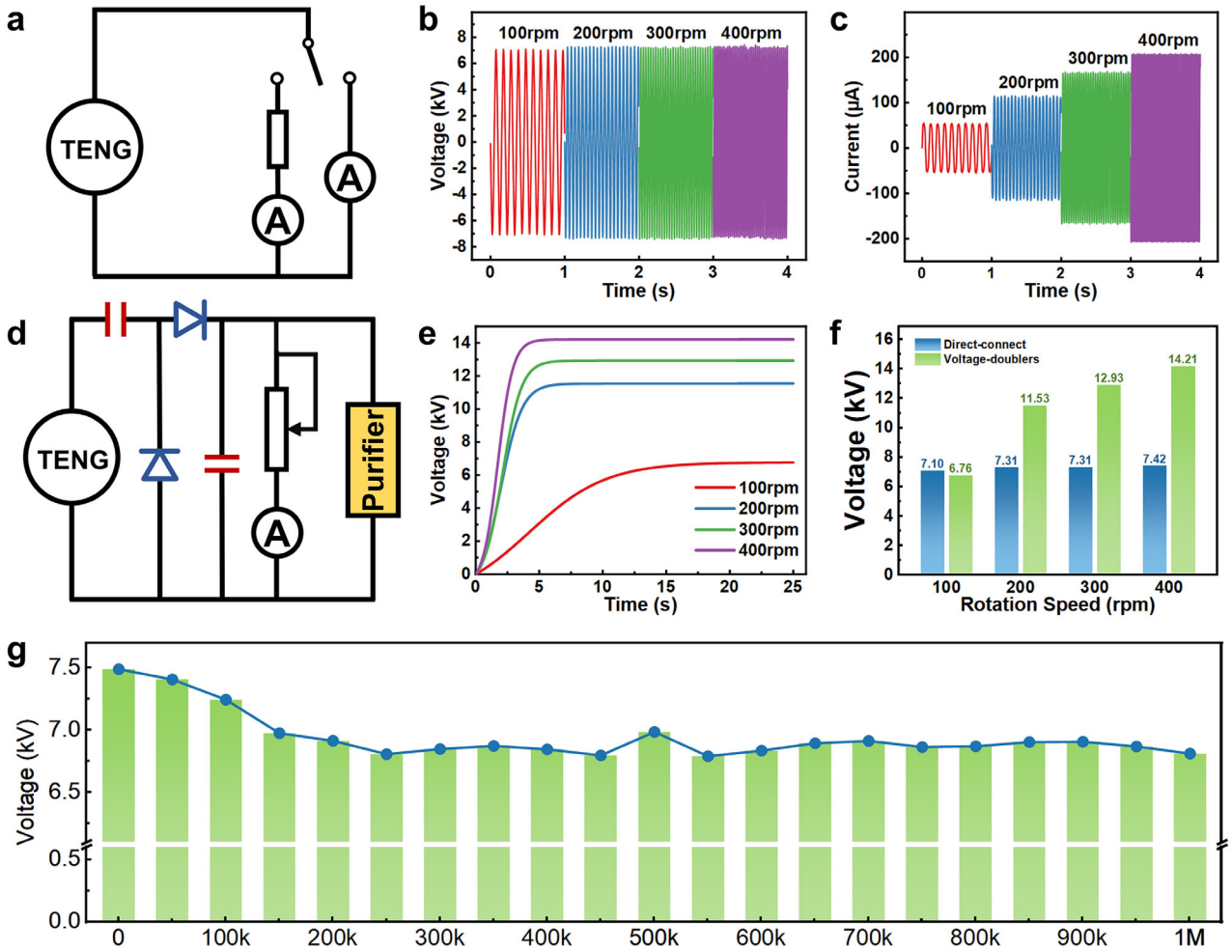

Figure 2. Electric characteristics of the FR-TENG. a) Measurement circuit for assessing the performance of the FR-TENG. b) Open-circuit voltage output at various rotation speeds. c) Short-circuit current output at different rotation speeds. d) Half-wave voltage doubler and its measurement setup. e) Voltage output of the half-wave voltage doubler. f) Comparative analysis of voltage output between the direct connection scenario and the half-wave voltage doubler configuration at varying rotation speeds. g) Durability test of FR-TENG with the operating for 1000000 cycles.

should be analyzed in two components: the oil fluid and the solid impurities.

According to electrohydrodynamics theory, the oil fluid satisfies the Navier–Stokes Equations (2 and 3):[43]

$$\rho\frac{\partial u}{\partial t}+\rho\ (u\cdot\nabla u)=\nabla\cdot\left[-pI+\mu\left(\nabla u+(\nabla u)^{T}\right)\right]+\rho g+F \tag{2}$$

$$\nabla\cdot u=0 \tag{3}$$

Here, ρ represents fluid density, p denotes pressure, μ stands for fluid viscosity, and u represents fluid velocity. Within the electrostatic oil purification process, the additional term F is described by the following Equation (4):[44]

$$F=\rho_e E-\frac{1}{2}E^2\nabla\varepsilon+\frac{1}{2}\nabla\left[E^2\rho\left(\frac{\partial\varepsilon}{\partial\rho}\right)_T\right] \tag{4}$$

This equation describes the force exerted by an external electric field on the oil fluid. As shown in the equation, the electric force is divided into three types of forces, namely the Coulomb force, the dielectric force, and the electrostrictive force. Since the oil fluid is incompressible and non-conductive, the charge in the oil can be neglected, so the first and third terms of the equation reduce to zero, leaving only the dielectric forces in effect.

Similarly, the force of the electric field on the solid impurities in the oil can be described similarly. However, different situations arise in this context. **Figure 3**a illustrates the possible forces on impurity particles during electrostatic oil purification. When an impurity particle moves directionally in an electrostatic oil purifier, it may be subjected to a combination of dielectric force (F_d) and Coulombic force (F_c) exerted by the electric field, along with viscous resistance (F_r) exerted by the oil.

For uncharged particles, the Coulomb force is zero. Consequently, the electric field force F_e acting on it can be expressed as follows:

$$F_e=F_d=-\frac{1}{2}E^2\nabla\varepsilon \tag{5}$$

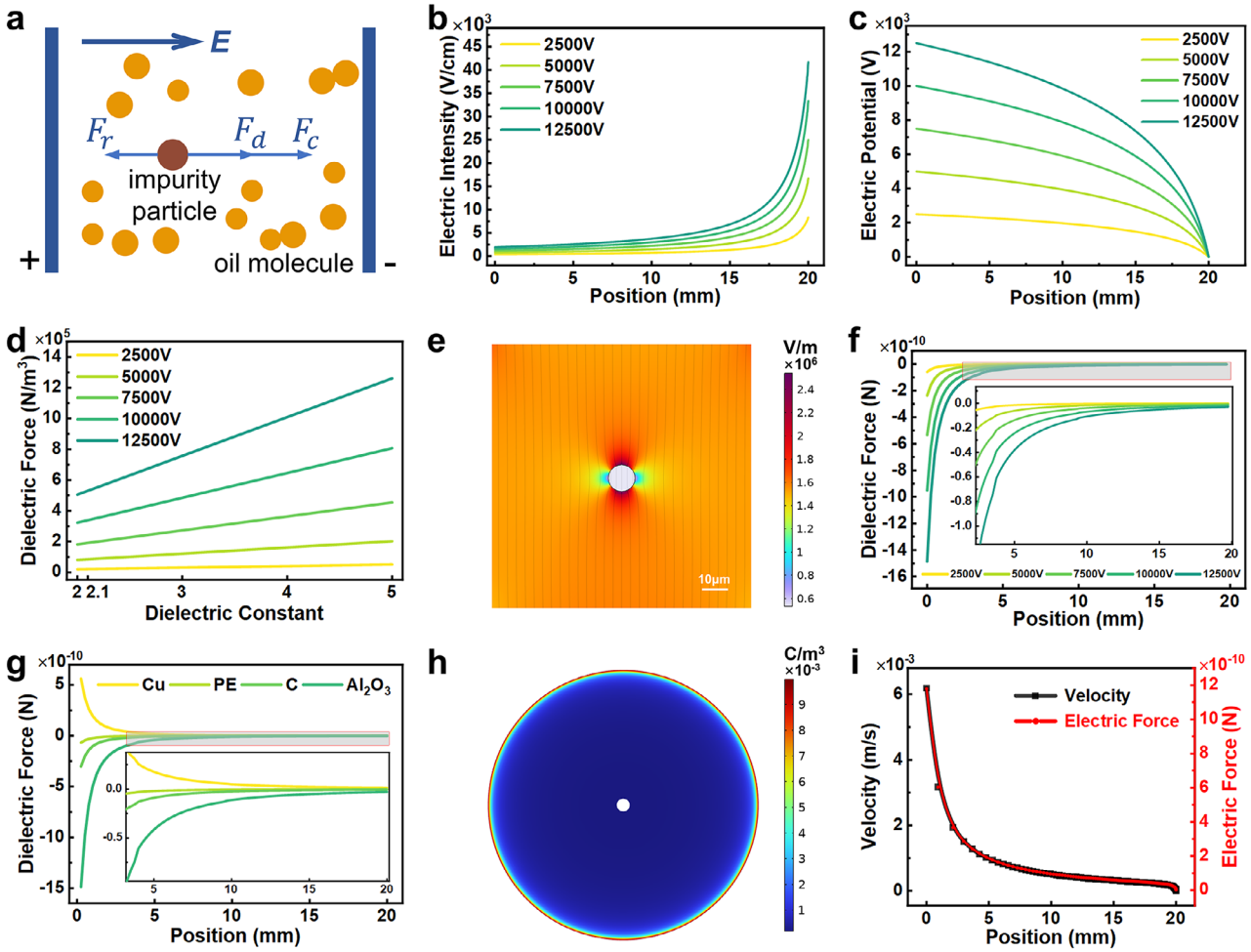

Figure 3. Simulation analysis of forces and kinematic performance of oil and solid particles during oil purification. a) force analysis of impurity particles under electric field action. b) variation curve of electric intensity with the position at different voltages. c) variation curve of electric potential with the position at different voltages. d) effect of voltage and dielectric constant on the dielectric force applied to the oil fluid. e) diagram of the electric intensity in the vicinity of a particle. f) dielectric force curves for particles at different positions and different voltages. g) dielectric force curves for different kinds of particles at different positions. h) Space charge distribution in the purifier. i) electric force and velocity curves for a particle at different positions.

Here, E represents the electric field, and ϵ denotes the dielectric constant. Essentially, the force exerted by the electric field on uncharged solid impurities primarily arises from the non-uniformity of the dielectric constant and the electric field. In electrohydrodynamic theory, it can be computed equivalently using the Maxwell stress tensor.

On the other hand, solid impurities in the oil often get charged due to particle frictional interactions, particle collisions, preferential adsorption of ions in the liquid, or dissociation of surface dissociative groups on the particles.[11] Regarding the influence of electric fields on charge characteristics of impurity particles, conductive and non-conductive impurities are governed by distinct mechanisms. In conductive impurities, directional migration of free electrons under applied electric fields induces charge separation, resulting in positive charge accumulation at one terminus and negative charge concentration at the opposing extremity. However, this electrostatic induction process does not alter the particle's net charge. For non-conductive impurities, although devoid of free charge carriers, partial charge displacement occurs through molecular polarization under external electric fields, establishing localized polar domains characteristic of electric dipoles. These induced dipolar interactions generate short-range dielectric forces between particles, while the overall charge quantity of individual particles remains conserved throughout the process.

Charged solid impurities in the oil experience additional Coulomb forces, leading to:

$$F_e = F_c + F_d = qE - \frac{1}{2}E^2\nabla\epsilon \tag{6}$$

Here, q denotes the charge carried by the solid particles. Additionally, these particles experience viscous resistance from the oil as they move under the influence of the electric field, quantified by Stokes Law:[45]

$$F_r = 6\pi\eta v a \tag{7}$$

Here, η represents the viscosity coefficient of the liquid, v denotes the velocity of the solid particles relative to the liquid, and a signifies the radius of the solid particles. The impurities within the oil, propelled by the electric field force, overcome viscous resistance to migrate toward the center of the container and are subsequently entrapped by the dust collector.

It should be emphasized that the charge quantity carried by impurity particles during the purification process is not maintained at a constant level. Variations in this parameter may be induced by multiple mechanisms including particle frictional interactions, particle collisions, preferential adsorption of ions in the liquid, dissociation of surface dissociative groups on the particles, or transient electrode contact events. Due to the technical limitations in achieving real-time charge monitoring of individual particles throughout the dynamic purification process, a predetermined charge value is typically assigned in computational simulations. The resulting simulation outcomes therefore represent particle motion analysis under fixed charge conditions.

Initially, the electric field and electric potential distribution of the purifier were simulated using a laminar flow model and an electrostatic model. Figure S1 (Supporting Information) provides a top view of the structure and dimensions of the purifier, labeled with dimensions and some annotations. Figures S2 and S3 (Supporting Information) illustrate the electric field strength and electric potential distribution within the purifier when a voltage of 2500 to 12500 V is applied across both ends of the electrode (with the inner electrode grounded). Figure 3b,c illustrate the variation of electric field strength and electric potential at different positions inside the purifier. As distance R_a (the distance from the inner electrode to the investigating position as shown in Figure S1, Supporting Information) increases, the electric field strength gradually increases, while the electric potential gradually decreases. This varying electric field results in a dielectric force of considerable magnitude. Figure S4 (Supporting Information) illustrates the distribution of dielectric forces exerted on the oil fluid by the electric field in the purifier. The electric field gradient is maximal near the inner electrode, resulting in a higher dielectric force acting on the oil fluid in the same direction as the electric field, directing toward the inner electrode.

The dielectric constant of typical oil ranges from 2 to 5. Figure 3d displays the maximum magnitude of the dielectric force on oil fluid within this range of dielectric constant at varying voltages. The dielectric force on the oil fluid increases with the increase in the dielectric constant. The dielectric force increases more rapidly with the dielectric constant as the voltage increases. The oil used in the subsequent experiments has a dielectric constant of 2.1. With a fixed dielectric constant, the dielectric force increases in proportion to the voltage.

Due to the significant disparity in size between the solid particles and the purifier, a combination of finite element and boundary element methods is utilized to analyze the dynamic behavior of the solid particles within the purifier. This approach decreases both the mesh density and computation time necessary for the simulation. Additionally, a level-set two-phase flow model is used to track changes taking place at the interface between the solid particles and the oil fluid.

Uncharged particles are only subjected to dielectric forces in the electric field. Figure 3e illustrates the distribution of electric intensity in the vicinity of a particle. The electric intensity is higher on both sides of the particle along the direction of the electric field lines, while it is lower on both sides of the particle in the direction perpendicular to the electric field lines. However, this does not apply to the distribution of electric intensity near the particle, as shown in Figure S5 (Supporting Information). The statement suggests that the dielectric force primarily acts in the direction parallel to the electric field. As illustrated in Figure S6 (Supporting Information), the dielectric force primarily acts at the interface between the particle and the oil fluid due to the maximum gradient of the dielectric constant at this interface. F_d represents the combined force of the dielectric forces on the inner and outer sides of the particle. If the dielectric force on the inner side is smaller than that on the outer side, F_d points toward the inner electrode, aiding in oil purification. Figure 3f illustrates the trend of the dielectric force on the particles as a function of their positions (with the dielectric constant taken as 10). This trend indicates that the dielectric force is strongest when the particles are closest to the inner electrode. The dielectric force increases rapidly within the 5 mm range as the position approaches the inner electrode. Similar to the performance in the oil fluid, this is determined by the gradient of the electric field. Furthermore, increasing the voltage has a significantly positive effect on the dielectric force.

Various types of particles were analyzed in this study, including copper (Cu), polyethylene (PE), carbon (C), and alumina (Al_2O_3) particles. They were chosen to simulate typical solid contaminants in lubricating/hydraulic systems: metallic wear debris (Cu), metal oxides (Al_2O_3), carbonaceous deposits (Carbon), and plastic particulates (PE). The corresponding dielectric constants are provided in Table S1 (Supporting Information). Figure 3g depicts the difference in dielectric force encountered by each type of particle. Specifically, the dielectric force on copper particles is directed toward the outer electrode, which is detrimental to oil purification. In contrast, the dielectric force on the remaining three kinds of particles is all directed toward the inner electrode. The dielectric force increases with the increasing dielectric constant. In the vicinity of the outer electrode, the dielectric force exerted on all particles is similar in magnitude and tends toward zero.

Charged particles are influenced by both dielectric and Coulomb forces. The dielectric force affects charged particles similarly to uncharged particles. Hence, only the effect of the Coulomb force will be discussed here. A fluid flow particle tracking model is introduced to track the motion of charged particles in the purifier. Initially, the space charge distribution in the purifier is simulated, and the results are shown in Figure 3h. In contrast to the distribution of the electric field gradient, the charge density is lower near the inner electrode and higher near the outer electrode. Such a charge distribution compensates for the small dielectric force near the outer electrode. Due to the high charge density, the particles are more easily to be charged near the outer electrode. Even if the dielectric force is small, it can be supplemented by the Coulomb force to prevent the inability to remove particles near the outer electrode.

Once the Coulomb force has been incorporated into the simulation, it is necessary to assign an initial cumulative charge to the particles. A particle is released from the outer electrode to simulate the electric force (the combined force of Coulomb force and dielectric force) and its resulting velocity. The variation of these two with particle position R_a is illustrated in Figure 3i. From the

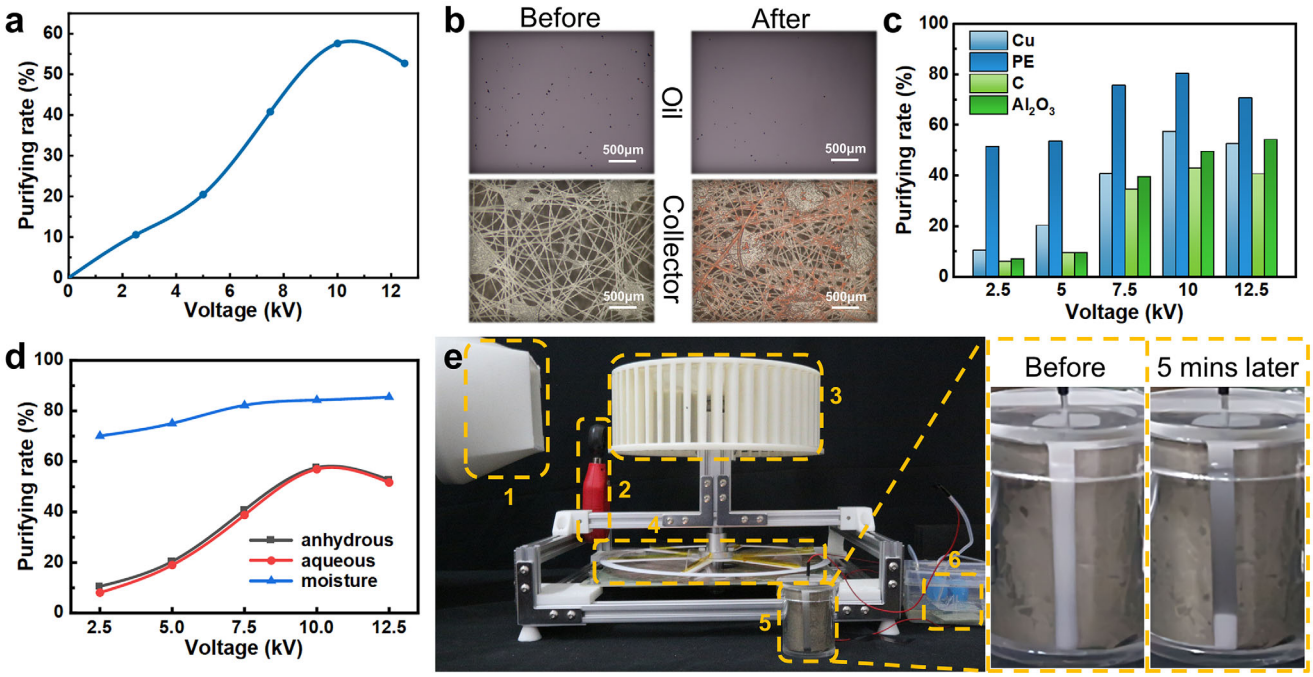

Figure 4. Purification performance of TEOP under different conditions. All experiments are conducted under ambient temperature and pressure conditions. a) Purification performance of TEOP on copper-containing oils at different voltages. b) Demonstration of TEOP's purification performance on copper-containing oils at a microscopic level. c) Purification performance of TEOP on oils with different particles. d) Comparison of the performance of TEOP in treating anhydrous and aqueous oils. e) Demonstration of wind-driven TEOP oil purification. 1 to 6 represent the blower, the anemometer, the wind turbine, the FR-TENG, the purifier, and the half-wave voltage doubler, respectively.

outer electrode to the inner electrode, the electric field strength and electric field gradient gradually increase, so the electric force increases as R_a decreases. The particle moves toward the inner electrode under the combined effect of electric force and viscous resistance. The velocity curve almost coincides with the electric force curve, indicating that the influence of electric force on the motion of the particle is much greater than that of viscous resistance. Thus, the purifier demonstrates high purification efficiency for charged particles.

The force and dynamic behavior of charged and uncharged contaminants under the influence of a DC electric field in the purifier are analyzed in detail through simulation. The theoretical insights from this simulation aim to inform subsequent performance research experiments of the purifier.

2.4. Purification Performance of TEOP

Four types of impurity particles were systematically selected to evaluate the TEOP purification performance, comprising Cu, PE, C, and Al_2O_3 particles. These materials were specifically chosen to represent typical solid contaminants encountered in lubricating/hydraulic oil systems: metallic wear debris, plastic particulates, carbonaceous deposits, and metallic oxides. The oil used is 45# transformer oil. Initially, the study focuses on the purification performance of copper powder, a common metal abrasive particle. Purification experiments are conducted on transformer oil containing copper powder at varying voltages, with each experiment lasting 15 min. The results are depicted in **Figure** 4a, which indicates that the purification rate peaks at 52.71% at 10 kV. Increasing the voltage beyond 10 kV decreases the purifying rate due to the instability, ionization, or dispersion of metal particles caused by high voltage. Figure 4b illustrates the oil and the dust collector's appearance before and after purification, demonstrating a significant reduction in suspended impurity particles in the oil and a considerable accumulation of impurity particles on the dust collector.

Similarly, experiments are conducted to purify transformer oil containing three additional types of particles under different voltages, and the purification results of the four types of particles are compared in Figure 4c. It is observed that as the voltage increases, the purification efficiency of the four types of particles also increases. The purification efficiencies of copper, PE, and carbon reach their peaks at 10 kV and then decline. This phenomenon may be attributed to the relatively low dielectric constants of these three particle types. When subjected to excessive voltage, over-polarization occurs, resulting in neutralization between positive and negative polarized charges, which consequently diminishes the net polarized charge. From a microscopic perspective, the excessively strong electric field induces molecular charge deflection beyond the maximum polarization position. This leads to weakened polarization phenomena, reduced effectiveness of the dielectric force, and ultimately a decline in purification efficiency. In contrast, the purification efficiency of alumina particles continues to rise. This is likely due to the higher dielectric constant of alumina, resulting in lower sensitivity to high voltage. A high dielectric constant corresponds to a higher polarization threshold, which requires higher voltages to trigger

over-polarization. However, in our experiments, the applied voltage of 12.5 kV remained below this threshold. As the voltage increases, both Coulomb forces and dielectric forces exhibit progressively enhanced effects, thereby sustaining continuous improvement in purification efficiency. Among all particles, PE achieves the highest purification efficiency 80.53% at 10 kV, primarily due to its low density, resulting in smaller particle mass for the same diameter. Simulation results indicate that the electric field force is independent of mass. Hence, PE exhibits the fastest movement under the electric field. Notably, although copper has the highest density, its purification efficiency surpasses that of C and Al_2O_3 particles. This may be attributed to the conductive nature of copper particles, which facilitates charge accumulation during purification. Specifically, under electrostatic induction, copper particles develop positive charges concentrated at one end and negative charges at the opposite end. Crucially, the magnitude of these bipolar charges on copper surfaces significantly exceeds the polarized charges generated on insulating impurity particles. This characteristic makes copper particles more likely to adsorb ions or charged dissociation groups in the oil, thereby becoming electrically charged. Consequently, the Coulomb force plays a more dominant role compared to the dielectric force, resulting in higher purification efficiency.

To validate the purification efficiency of TEOP on aqueous oil samples, experiments are conducted on copper-containing oil samples with moisture content up to 10%. The results are shown in Figure 4d. The effect of voltage on aqueous oil samples is consistent with that on anhydrous oil samples. The particle purification curve for samples containing 10% moisture content is nearly identical to that for anhydrous samples. The particle purifying rate exhibits a slight decline compared to that of anhydrous samples. During the experiment, small water droplets undergo coalescence and settle under the influence of the electric field. As the water droplets settle, they carry some solid particles to the bottom of the purifier. Due to the frictional resistance exerted on these particles by the bottom, they cannot be purified effectively. However, this does not significantly impact the efficiency of TEOP in purifying aqueous oil. In other words, TEOP maintains good purification effects even in treating oils with a moisture content of up to 10%. This is nearly 100 times higher than the 1000 ppm moisture content limit of traditional electrostatic oil purifiers. Furthermore, TEOP is capable of separating water from aqueous oil samples while purifying solid impurities. At an applied voltage of 10 kV, where the highest purifying rate for solid particles is achieved, TEOP achieves a water purifying rate of 84.28%. The water purifying rate by TEOP increases with the applied voltage.

Comparative analysis with existing electrostatic oil purification systems is essential to evaluate the performance of the TEOP. As summarized in Table S2 (Supporting Information), key parameters (e.g., operating condition, purification duration, moisture limit, and purification efficiency) are systematically compared across representative systems. In this study, experiments are conducted under static conditions. Prior to electrification, oil samples are thoroughly agitated to achieve homogeneous particle suspension. Post-experiment observations reveal partial particle sedimentation at the container bottom. Due to the enhanced frictional resistance exerted on settled particles, which significantly restricts their mobility under the electric field compared to suspended particles, the period of fastest purification spanned from device power activation until the natural sedimentation of the majority of particles. Notably, in purification efficiency calculations, settled particles are categorized as unpurified, leading to comparatively lower measured efficiency values. In contrast, other systems employ dynamic configurations where recirculation pumps continuously maintain particle suspension to optimize electric field utilization. The operational disparity between static and dynamic systems theoretically implies substantial potential for efficiency enhancement in the TEOP method. Future work will integrate dynamic recirculation mechanisms into the TEOP system to sustain electric field efficacy throughout the purification process.

It is noteworthy that the TEOP can be driven by ambient energy. Figure 4e presents a demonstration experiment of a wind-driven TEOP oil purification system. The FR-TENG can be converted to wind-driven by attaching a wind turbine to its rotor shaft. The wind turbine converts wind energy into mechanical energy to drive the rotor, generating a high-voltage output. This output is then converted into DC by a circuit to create a high-voltage inhomogeneous DC field in the purifier. Part of the rotor structure is modified to reduce the starting torque of the FR-TENG. In the demonstration experiments, the airflow generated by a blower simulates natural wind, and an anemometer measures the wind speed. Figure 4e depicts a comparison of the oil samples before purification and after 5 min of wind purification. The upper layer of clear liquid in the purifier is the anhydrous oil sample after separating the water. Video S1 (Supporting Information) depicts the complete process of the demonstration experiment conducted at wind speeds of ≈6 ms^{-1} (equivalent to a wind force of 4). The TEOP is initiated from a standstill by the wind force, purifying the aqueous and copper-containing oil samples within the purifier. The starting wind speed can be reduced by optimizing the wind turbine and rotor structure.

3. Conclusion

In this study, a self-powered triboelectric electrostatic oil purifier (TEOP) is proposed, capable of simultaneously separating and purifying solid impurities and water from oil samples with high moisture content. By collecting ambient energy through an FR-TENG, the system generates a high-voltage AC output, which is converted into a higher DC electric field via a circuit, assisting in the separation of solid impurities with the aid of a dust collector. To explore the motion characteristics of solid particles under a high-voltage DC field, a coupled model incorporating laminar flow, level-set two-phase flow, and particle tracking is utilized to simulate the forces and motion of solid impurities in oil. The simulation results indicate that TEOP can achieve rapid purification through the combined effect of dielectric and Coulomb forces, alongside the dust collector. Furthermore, experimental results validate TEOP's purification performance under various conditions. Among the four particles, PE achieves the highest purification efficiency 80.53% at 10 kV. Notably, the particle purification curve for samples containing 10% moisture content is nearly identical to that for anhydrous samples, showing high stability and effectiveness. This represents a nearly 100-fold increase in the permissible moisture content compared to traditional electrostatic oil purifiers, where the moisture limit is typically below 1000 ppm. By integrating a wind turbine onto the shaft of the

FR-TENG, TEOP can leverage wind energy to drive purification. The start-up wind speed is as low as 6 ms^{-1}. These findings highlight the significant potential of TEOP to utilize ambient energy for oil purification, providing a highly adaptive, sustainable, and efficient solution for industrial oil treatment.

4. Experimental Section

Fabrication of the FR-TENG: The FR-TENG used in this study comprises two primary components: the stator and the rotor. The stator base, fabricated via a printed circuit board (PCB) process, is 1.6 mm thick and features a grid of alternating copper electrodes with 8 mm spacing. A 50 μm thick nylon film was applied over the electrode surface, functioning as the electropositive triboelectric layer. The rotor was constructed from a 4 mm thick laser-cut acrylic disk with an outer diameter of 320 mm and an inner diameter of 20 mm. The disk includes six equally spaced radial slots, each 1 mm wide and 107.5 mm long, containing a 100 μm thick PVC film, which was secured by Kapton tape. This PVC film, acting as the electronegative triboelectric layer, possesses sufficient malleability to ensure effective contact between the triboelectric layers during the operation of the FR-TENG.

Measurement of the Electrical of FR-TENG: A Keithley 6514 electrometer, with an internal resistance of ≈200 TΩ, was used for power measurements. The device allows selection between voltage and current measurements by switching ranges.

Measurement of the Particle Concentration and Moisture Content In Oil: The particle concentration in the oil was determined by counting particles on a counter slide using an electron microscope. Moisture content was measured with a Byes-8 Karl Fischer Moisture Titrator, which utilizes the Karl Fischer Coulomb titration method. The titrator features a measurement range of 3 μg to 100 mg, a sensitivity of 0.1 μg, and an accuracy of ±2 μg for measurements between 3 μg and 1 mg.

Demo Capture and Wind Speed Measurement: The camera used for the shooting is a CANON EOS 5D Mark II, and the microscopic images were captured with a CCD microscope.

Supporting Information

Supporting Information is available from the Wiley Online Library or from the author.

Acknowledgements

X.W. and M.S. contributed equally to this work. This work was supported by the Ministry of Science and Technology of the People's Republic of China [Grant No. 2021YFA1201600]; and the National Natural Science Foundation of China [Grant No. 52371345].

Conflict of Interest

The authors declare no conflict of interest.

Data Availability Statement

Research data are not shared.

Keywords

dehydration, electrostatic oil purification, particle removal, sustainable, triboelectric nanogenerator

Received: October 20, 2024
Revised: March 7, 2025
Published online:

[1] Y. Hsu, C. Liu, *Environ. Monit. Assess.* **2011**, *176*, 197.
[2] G. K. Irungu, A. O. Akumu, J. L. Munda, in *2016 IEEE Electrical Insulation Conference (EIC)*, IEEE, Montreal, QC, Canada, **2016**, pp. 174–177.
[3] K. Parekh, R. Radadiya, R. Gaur, S. Shahabuddin, I. Ahmad, *Int. J. Environ. Sci. Technol.* **2023**, *20*, 12323.
[4] X. Ye, J. Wang, W. Shi, *J. Coastal Res.* **2019**, *94*, 249.
[5] H. Yanada, Y. Daiou, Y. Ogi, *J. Electrost.* **2012**, *70*, 117.
[6] K. O. Boadu, O. F. Joel, D. K. Essumang, B. O. Evbuomwan, *Chem. Sci. Int. J.* **2019**, *26*, 1.
[7] S. Sarkar, D. Datta, K. S. Deepak, B. K. Mondal, B. Das, *J. Mater. Cycles Waste Manage.* **2023**, *25*, 1935.
[8] L. Safiddine, H. Zafour, U. M. Rao, I. Fofana, *Energies* **2019**, *12*, 368.
[9] A. Ilyushchanka, I. Charniak, A. Kusin, R. Kusin, I. Zakreuski, E. Eremin, *J. Phys. Conf. Ser.* **1260**, *2019*, 062010.
[10] T. T. Vu, T. V. La, V. T. Pham, T. G. Vu, *Arabian J. Chem.* **2022**, *15*, 103683.
[11] H. Yanada, S. Takagi, S. Mamiya, *J. Electrost.* **2015**, *74*, 1.
[12] K. D. Tran, Y. Kojima, Y. Terashita, H. Yanada, *Proc. of the JFPS Int. Symp. Fluid Power.* **2008**, *2008*, 335.
[13] Z. L. Wang, *ACS Nano.* **2013**, *7*, 9533.
[14] F. Fan, Z. Tian, Z. L. Wang, *Nano Energy.* **2012**, *1*, 328.
[15] Z. L. Wang, *Mater. Today.* **2017**, *20*, 74.
[16] S. Pan, Z. Zhang, *Friction* **2019**, *7*, 2.
[17] A. Kulandaivel, S. Potu, R. K. Rajaboina, U. K. Khanapuram, *ACS Appl. Mater. Interfaces.* **2024**, *16*, 58029.
[18] S. Potu, A. Kulandaivel, B. Gollapelli, U. K. Khanapuram, R. K. Rajaboina, *Mater. Sci. Eng. R: Rep.* **2024**, *161*, 100866.
[19] R. K. Rajaboina, U. K. Khanapuram, A. Kulandaivel, *Adv. Sens. Res.* **2024**, *3*, 2400045.
[20] R. Zhang, Q. Xu, S. Bai, J. Hai, L. Cheng, G. Xu, Y. Qin, *Nano Energy.* **2021**, *79*, 105434.
[21] S. Niu, Y. Liu, X. Chen, S. Wang, Y. S. Zhou, L. Lin, Y. Xie, Z. L. Wang, *Nano Energy.* **2015**, *12*, 760.
[22] J. Chen, Z. L. Wang, *Joule* **2017**, *1*, 480.
[23] X. Xie, Y. Zhang, C. Chen, X. Chen, T. Yao, M. Peng, X. Chen, B. Nie, Z. Wen, X. Sun, *Nano Energy.* **2019**, *65*, 103984.
[24] K. Xia, D. Wu, J. Fu, Z. Xu, *Nano Energy.* **2020**, *77*, 105112.
[25] H. L. Wang, Z. H. Guo, G. Zhu, X. Pu, Z. L. Wang, *ACS Nano.* **2021**, *15*, 7513.
[26] S. R. Begum, A. Chandrasekhar, *ACS Appl. Electron. Mater.* **2023**, *5*, 1347.
[27] Y. Bai, H. Feng, Z. Li, *Cell Rep. Phys. Sci.* **2022**, *3*, 101108.
[28] J. Sun, L. Zhang, S. Gong, J. Chen, H. Guo, *Nano Energy.* **2024**, *119*, 109010.
[29] D. Sun, W. Song, C. Li, T. Chen, D. Zhang, J. Zhang, S. Ramakrishna, Y. Long, *Nano Energy.* **2022**, *101*, 107599.
[30] Y. Guo, H. Zhang, Y. Zhong, S. Shi, Z. Wang, P. Wang, Y. Zhao, *ACS Appl. Mater. Interfaces.* **2023**, *15*, 5242.
[31] J. Zhang, P. Chen, L. Zu, J. Yang, Y. Sun, H. Li, B. Chen, Z. L. Wang, *Small* **2022**, *18*, 2202835.
[32] F. Li, C. Deng, M. Sun, X. Wan, S. Sun, W. Xu, T. Du, Y. Zou, H. Yuan, X. Pan, J. Mi, M. Xu, *Nano Energy.* **2023**, *112*, 108459.
[33] Z. Wang, Y. Shi, F. Liu, H. Wang, X. Liu, R. Sun, Y. Lu, L. Ji, Z. L. Wang, J. Cheng, *Nano Energy.* **2020**, *74*, 104910.
[34] J. He, X. Guo, C. Pan, G. Cheng, M. Zheng, Y. Zi, H. Cui, X. Li, *Nanotechnology* **2023**, *34*, 385403.
[35] D. Yang, Y. Feng, B. Wang, Y. Liu, Y. Zheng, X. Sun, J. Peng, M. Feng, D. Wang, *Nano Energy.* **2021**, *90*, 106641.
[36] D. Wang, Z. Liu, X. Dong, D. Zhang, X. Chen, *Chem. Phys. Lett.* **2023**, *830*, 140795.
[37] R. Lei, Y. Shi, Y. Ding, J. Nie, S. Li, F. Wang, H. Zhai, X. Chen, Z. L. Wang, *Energy Environ. Sci.* **2020**, *13*, 2178.

[38] Z. Qu, J. Cao, C. Shan, Z. Zhang, G. Cheng, J. Ding, *Nano Energy.* **2022**, *100*, 107497.
[39] F. Li, X. Wan, J. Hong, X. Guo, M. Sun, H. Lv, H. Wang, J. Mi, J. Cheng, X. Pan, M. Xu, Z. L. Wang, *Adv. Mater. Technol.* **2022**, *7*, 2200198.
[40] A. Sasaki, *Proc. Inst. Mech. Eng., Part J.* **2006**, *220*, 471.
[41] Y. Shen, E. Elele, B. Khusid, *Electrophoresis* **2011**, *32*, 2559.
[42] S. H. Park, L. Katzir, D. Shmilovitz, in *2015 17th Euro. Conf. Power Electronics and Applications (EPE'15 ECCE-Europe)*, IEEE, Geneva, Switzerland, **2015**, pp. 1–7.
[43] O. Lastow, W. Balachandran, *J. Electrost.* **2006**, *64*, 850.
[44] H. H. Woodson, J. R. Melcher, in *Electromechanical Dynamics*, John Wiley And Sons, INC. , New York, **1968**, pp. 330–417.
[45] P. C. F. Pau, J. O. Berg, W. G. McMillan, *J. Phys. Chem.* **1990**, *94*, 2671.